Formation mechanism and elimination of mesophase in AlN powder synthesized in a carbothermal reduction nitriding process

Xin Wei [1], Hao Zhang [2], Dengqiong Sun [2], Chenguang Tian [2], Jun Guo [2], Song Cui [3], Wenming Tang [1, *]

(1. School of Materials Science and Engineering, Hefei University of Technology, Hefei 230009, China;

2. Hefei Shengda Electronic Technology Industry Co. Ltd., Hefei 230088, China;

3. 43rd Institute of China Electronics Technology Group Corporation, Hefei 230088, China)

Abstract: A mesophase of Al_2OC was first determined in the AlN powder synthesized in batch quantities via a carbothermal reduction nitridation (CRN) process. The formation mechanism of the mesophase was described. Finally, the CRN process parameters were optimized to eliminate the mesophase in the AlN powder. The results show that as an incomplete reduction product of Al_2O_3, Al_2OC has a highly similar crystal structure to AlN. The formation of Al_2OC depends on the P_{N2} and P_{CO} in the synthetic furnace. At the conditions of T = 1700 °C, P_{N2} = 10^{-5} kPa, and P_{CO} = $10^{-0.008}$-$10^{0.973}$ kPa, the formation of Al_2OC is thermodynamically favorable. By increasing the flow rate of N_2 in the synthetic furnace, the formed Al_2OC was unstable and decomposed into AlN. Hence, the C and O contents of the AlN powder synthesized in batch quantities were greatly reduced. It can significantly improve the performance of the AlN ceramics.

Keywords: Synthesis of inorganic materials, carbothermal reduction nitridation (CRN), mesophase, thermodynamics, microstructure

* Corresponding author. Tel. & Fax: +86 551 62901362.

E-mail address: wmtang@hfut.edu.cn (W.M. Tang).

1. Introduction

Due to its high thermal conductivity (up to 320 W/(m·K) in theory), low thermal expansion coefficient matched with semiconductor materials such as Si and GaAs (4.2 × 10^{-6} /K, Si and GaAs: 3-4 × 10^{-6} /K, 25-200 °C), low dielectric constant (1 MHz, 8.0) and dielectric loss, as well as good electrical insulation properties, aluminum nitride (AlN) has become one of the most ideal ceramic substrates and electronic packaging materials [1-3]. High-property AlN ceramic substrates cannot be fabricated without high-quality AlN powder raw materials of high N concentration and low O and C concentrations. Currently, the carbothermal reduction nitridation process (CRN) is the mainstream technology used around the world [4-6] for synthesizing AlN powder in batch quantities. Other techniques such as direct nitridation, self-propagating high temperature synthesis and sol-gel method have been also widely used [7-10].

The CRN process in AlN powder synthesis is carried out in terms of a gas-solid reaction, including two sub-processes of the reduction reaction of Al_2O_3 by C and the reaction of the reduction products with N_2 to form AlN [11]. In detail, as the reaction temperature increases above 1500 °C, the reaction between the carbon black and the Al_2O_3 powder takes place to produce vapors of Al(g) and/or low-valent oxides of Al, such as Al_2O(g). The reduction products of Al(g) and/or Al_2O(g) have high reactivity and react rapidly with N_2 to synthesize AlN [12]. The concentrations of the C and O impurities are the main factors affecting the quality of the synthesized AlN powder. Generally, the C impurity content in the AlN powder comes from residual carbon black [13], while the O impurity content is derived from the residual Al_2O_3 and O

atoms dissolved in the AlN crystal lattice in the CRN process [14]. The O atoms dissolved in the AlN crystal lattice occupy the N atom positions, which induce Al vacancies and generates a strong phonon scattering effect. The thermal conductivity of the AlN ceramics is therefore sharply reduced [15]. Almost no other sources of C and O impurities have been reported in the CRN process.

Regarding the solid-state reaction process, if the thermodynamic and kinetic driving forces of the reaction are inadequate, one or more mesophases will be formed. Using the reduction reaction of Al_2O_3 with C as an example, Al_4C_3 is first formed, and then it reacts with Al_2O_3 to form Al_2OC and/or Al_4O_4C [16]. AlN powder is synthesized by the CRN process employing C and Al_2O_3 as the main raw materials. It is unknown which of the following compounds, Al_2OC, Al_4O_4C, or Al_4C_3, acts as the mesophase in the CRN process, so far. If these mesophases form in the CRN process and exist in the AlN powder, the O and C concentrations of the AlN powder are highly increased and the N concentration of the AlN powder is decreased, accordingly. The quality of the AlN powder is therefore highly degraded. It is of great value to study the formation and characteristics of the mesophase in the AlN powder synthesized by the CRN process both theoretically and industrially.

In the current work, high-purity and ultrafine Al_2O_3 powder and nanoscale carbon black are used as raw materials to prepare AlN powder in batch quantities via the CRN process. Taking the AlN powder of low N content and high C and O contents as samples, its composition, morphology, crystal structure, and phases were investigated to identify the mesophase in the AlN powder. Furthermore, the formation mechanism

and condition of the mesophase was determined via thermodynamic calculations. Accordingly, an improved process plan was proposed to eliminate the mesophase in the AlN powder in the CRN process. Finally, the AlN powders of different C and O contents synthesized in this work were used as raw materials to prepare bulk AlN ceramics via a commonly-used process of tape casting and subsequently pressureless sintering [17, 18]. The thermal conductivities and bending strengths of the AlN ceramics were mainly concerned to verify the significant improvement of the AlN ceramic performance by reducing the C and O contents through eliminating the mesophase in the AlN powder. This study is believed to provide important background for the production of high-quality AlN powder in the CRN process, both theoretically and experimentally.

2. Material and methods

2.1 Synthesis of the AlN powder

TABLE 1 Characteristics of ultrafine Al_2O_3 and nanoscale carbon black powders

	Al_2O_3	Carbon black
Purity / %	99.9	99.9
Specific surface area / (m^2/g)	8.9	75.0
Average particle size (d_{50}) / μm	0.500	0.042

The raw materials used in this work include high-purity, ultrafine Al_2O_3 powder and nano carbon black powder, purchased in China National Pharmaceutical Industry Corporation Ltd. Characteristics of the two types of powders are shown in Table 1.

The organic binder used in this study was analytically pure, also purchased in China National Pharmaceutical Industry Corporation Ltd.

The Al_2O_3 powder and nano carbon black powder were blended at a mass ratio of 1:3.5 and dry-milled for 5 h in a planetary ball mill at a speed of 300 rounds/min. Both the jar and milling balls were made of 99.9 wt% corundum ceramics. 5 wt% organic binder was poured into the powder mixture and then uniformly stirred into plasticine. Next, the plasticine was extruded into short rods, and finally, the plasticine rods were placed in an atmosphere protecting furnace and annealed at 360 °C for 2 h at a rate of 120 °C/h. The adhesive-discharging process was carried out in a 99.99 vol% high-purity N_2 atmosphere at a gas flow rate of 15 L/min.

After that, the synthesis precursors of AlN powder were prepared. The precursor rods were shifted into a high temperature synthesis furnace with a batch capability of 5 kg AlN powder per hour. The precursors were calcined at 1700 °C for 12 h at a heating rate of 100 °C/h. After that, the furnace was cooled to 300 °C at a rate of 100 °C/h and then naturally cooled to room temperature. The calcination process was carried out under the protection of the 99.99 vol% high purity N_2 gas at a gas flow rate of 250 L/min. The short rod-shaped AlN calcined products were then placed in a decarburization furnace and annealed at 700 °C for 2 h in air at a heating rate of 100 °C/h. After that the furnace was cooled to 300 °C at a rate of 100 °C/h and then naturally cooled to room temperature. After pulverizing, the AlN powder final product was achieved.

2.2 Preparation of the AlN ceramics

TABLE 2 Adhesive evacuating and sintering parameters of the AlN green pieces

Processing	Temperature range /℃	Heating rate /(℃/min)	Holding time /min
Adhesive evacuating	R.T.-170	1.3	/
	170-350	0.75	/
	350-500	0.83	/
	500-580	0.8	30
Sintering	R.T.-1300	10	/
	1300-1800	5	240

The organic binder, dispersant, plasticizer and solvent were dissolved in absolute ethanol. The powder mixture of AlN and 5 wt% Y_2O_3 sintering additives were then added into the solution and sealed in a corundum jar. The corundum balls of 10 mm in diameter were used as the milled medium. The mixture was milled for 48 h at a speed of 50 rounds/min, till a uniform slurry was obtained. After tape casting, stacking, and cold isostatic pressing at 20 MPa, the AlN green pieces were made. And then, the adhesive evacuating of the AlN green pieces was performed. The main process parameters were listed in Table 2. Finally, the AlN green pieces were sintered in a graphite furnace at 1800 ℃ for 4 h. The main sintering process parameters were also listed in Table 2. After that, the AlN ceramics were cooled to 1300 ℃ at a rate of 5 ℃/min, and then cooled to room temperature with the furnace. The whole adhesive evacuating and sintering processes are protected under a flowing N_2 atmosphere at a rate of 200 L/min.

2.3 Characterization

The O, N and C contents of the as-calcined, as-decarburized, and as-pulverized AlN powder were detected using an ON836 type oxygen-nitrogen content analyzer and a CS844-MC type carbon content analyzer, respectively. For each test, at least three samples were employed to obtain the average value. In the as-decarburized products, dark grey particles were chosen and dry ground in an agate mortar to prepare the powder sample. A SU8020 type field emission scanning electron microscopy (FE-SEM) equipped with an Oxford INCA type energy dispersive spectrometer (EDS) was used to observe the powder morphology and its micro-zone compositions. Due to the poor conductivity of the powder sample, gold spraying was necessary before SEM observation. The gold spraying parameters were set as 35 mA for 90 s. Phases of the powder sample was analyzed using an X'Pert PRO MPD type X-ray diffractometer (XRD) with a Cu target (Kα, λ=0.154 nm), and the tube voltage and current were 40 kV and 40 mA, respectively. The scanning rate was set as 0.02° per 20 s and the scanning angle range (2θ) was from 10° to 90°. An ESCALAB250xi type X-ray photoelectron energy dispersive spectrometer (XPS) was employed for qualitative and quantitative analysis of the elemental valences of the powder sample. A JEM-2100F type field emission high-resolution transmission electron microscopy (HRTEM) equipped with an energy dispersive spectrometer (EDS) was used to observe and analyze the morphology, composition distribution, and crystal structure of the powder sample. Before the TEM analyses, the powder sample was first ground for 10 min, ultrasonically dispersed in alcohol, dropped on a carbon film, and finally glued on a copper net. By the way, for the planar spacing measurement, three points were tested

to calculate the average value.

The densities of the sintered AlN ceramic specimens were determined by the Archimedes method. The phases of the AlN specimens were identified by XRD, using the same test parameters above. The thermal conductivities of the AlN specimens of 10 mm×10 mm×2 mm in shape were measured at room temperature, employing an LFA447 type laser thermal conductivity meter. The bending strengths of the AlN specimens of 40 mm×3 mm×2 mm in shape were measured in accordance with the China national standard GB/T 6569-2006 (ISO14704:2000) "Fine ceramics test method for flexural strength of monolithic ceramics at room temperature". The test was conducted using an AG-X PLUS type microcomputer control electronic universal testing machine with a testing span of 30 mm and a beam displacement rate of 0.5 mm/min. The bending fracture morphologies and microzone compositions of the AlN specimens were tested by SEM and EDS, respectively.

3 Results and Discussion

3.1 Morphologies and compositions of the AlN powder

After calcination at 1700 °C for 12 h and then decarbonization, most of the AlN products were light grey on the outside and at the fracture surfaces. However, a small amount of unsatisfactory AlN products exist with dark grey outer and fracture surfaces (Figure 1).

FIGURE 1 Two types of rod-like AlN samples after calcination and decarbonization

TABLE 3 O, N and C contents of two types of AlN samples after calcination and decarbonization

Sample	O/(wt%)	N/(wt%)	C/(ppm)
Slight grey 1	0.61	33.55	398
Slight grey 2	0.63	33.54	436
Slight grey 3	0.68	33.48	445
Ave.	0.64	33.52	426
Dark grey 1	0.82	33.36	996
Dark grey 2	0.88	33.31	1088
Dark grey 3	0.97	33.27	1257
Ave.	0.89	33.31	1114

As shown in Table 3, after calcination and decarburization, the light grey AlN sample is stable in composition with low O and C contents and high N content, indicating that the synthesis reaction for the AlN products is complete in the CRN process, and the decarburization effect is satisfactory. In comparison, the dark grey sample has low N content and significantly higher O content than the former. Also, the C content of the dark grey sample is about two times higher than that of the light grey sample. It is obvious that there are impurities containing C and O in the dark grey AlN products.

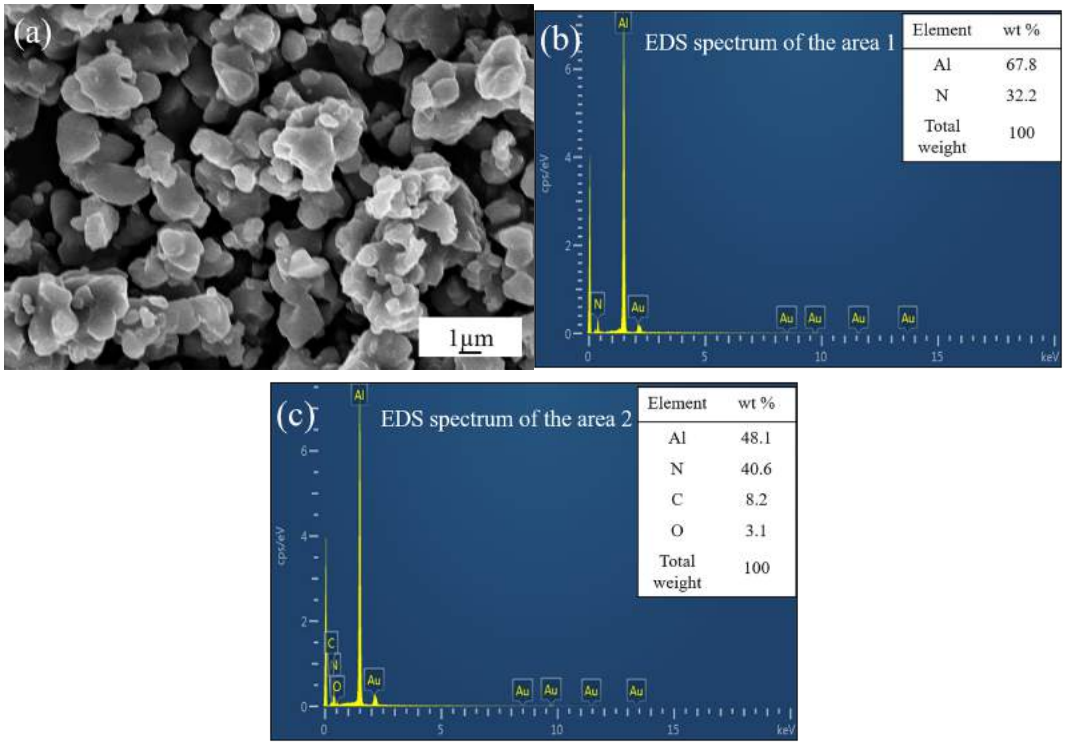

FIGURE 2 SEM planar image and EDS spectra of dark grey AlN powder sample: (a) SEM image; (b) and (c) EDS spectra of square areas 1 and 2 in Figure a, respectively

The surface morphology of the dark grey AlN powder sample is shown in Figure 2a. The AlN particles are mostly spherical, where a portion agglomerate to form big secondary particles. EDS tests show that the smooth particle contain only Al and N elements (Figure 2b), corresponding to pure AlN particles. In contrast, the rougher particles contain higher C and O contents, along with the Al and N elements (Figure 2c). In these samples, C and O impurities exist, due to the incomplete synthesis of AlN.

3.2 *Mesophase*

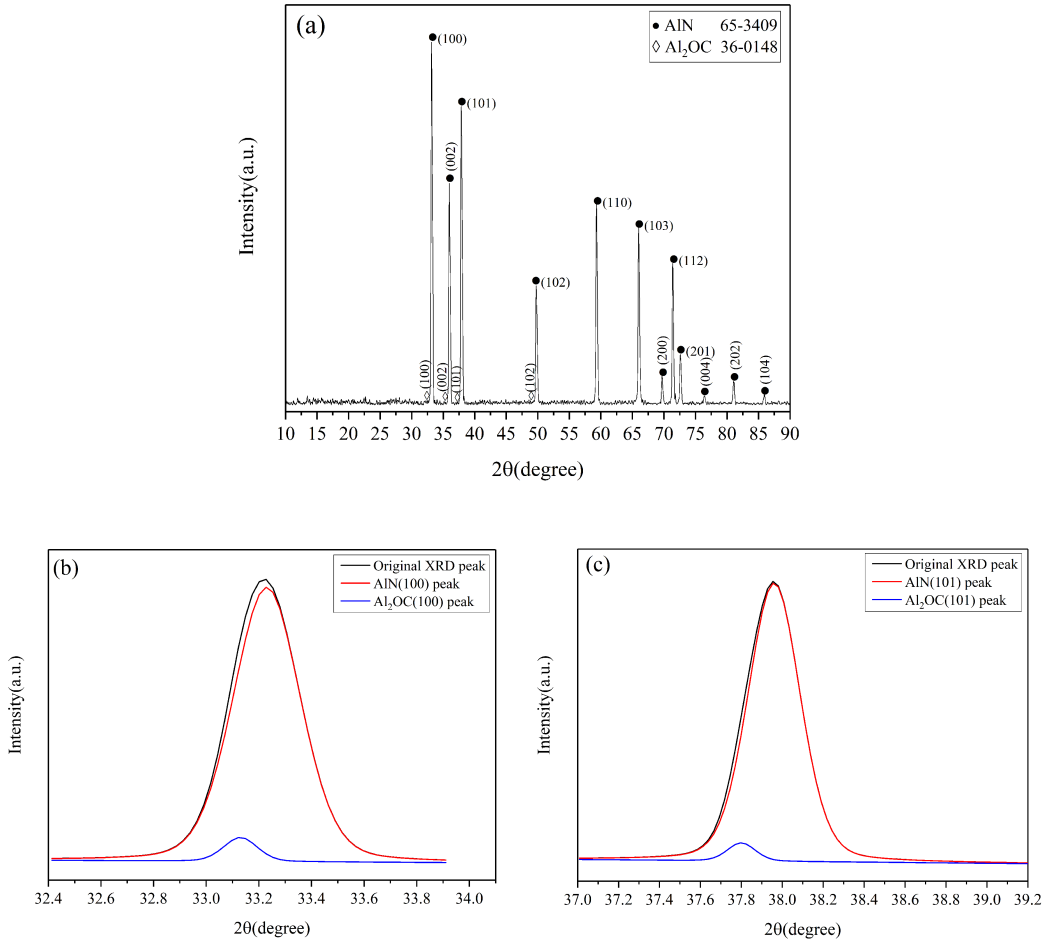

FIGURE 3 (a) XRD pattern of the dark grey AlN powder sample; (b) and (c) Differentiating-imitations of the diffraction peaks situated at 2θ=32.4º-34º and 37-39.2º, respectively

To determine the phase composition of the dark grey AlN powder sample, an XRD analysis of the sample was performed, and the results are shown in Figure 3a. The main phase of the dark grey AlN powder sample is AlN. However, 2θ values of the three strong peaks of the AlN phase in Figure 3a were shifted left by 0.01-0.02º, comparing with the standard XRD pattern of AlN (PDF65-3409). This indicates that diffraction peak overlapping of AlN and other phases may occur. In fact, the

diffraction peaks of Al_2OC (100) (2θ = 33.13º) and Al_2OC (101) (2θ = 37.80º) are very close to those of AlN(100) and (101) with a slight leftward shift. Therefore, it was predicted that the AlN diffraction peaks in Figure 3a were constructed by the diffraction peaks of AlN and Al_2OC. Accordingly, taking the strongest peak (2θ = 33.25º) and second-strongest peak (2θ = 37.97º) in Figure 3a as examples, two differentiated and imitated diffraction peaks, referring to the AlN and Al_2OC (100) and (101) planes, are shown in Figure 3b and c, respectively. Since the intensity of the AlN diffraction peak is so high and that of the Al_2OC diffraction peak is so weak in Figure 3b and c, the Al_2OC in the dark grey AlN powder sample is a low-concentration impurity phase.

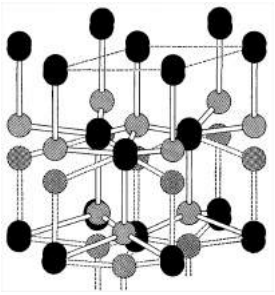

FIGURE 4 Al_2OC crystal structure schematic in which the black circles are the C, O atoms, and the others are the Al atoms [19]

In the Al-O-C ternary system, there are two ternary compounds, i.e., Al_2OC and Al_4O_4C [20]. Between them, Al_2OC has a similar wurtzite-type crystal structure to AlN, and the formation of Al_2OC can be achieved through N atom replacement in the AlN crystal lattices with C and O atoms (Figure 4) [19, 21, 22]. As reported by Qiu et al. [23], a solid solution between Al_2OC and AlN should be formed in the Al_4C_3-AlN-Al_2O_3 ternary system. The defect reaction equation for this process can be described as follows:

$$2AlN \xrightarrow{Al_2OC} 2Al_{Al} + N_C^{\bullet} + N_O' \quad (1)$$

When 2 mol AlN dissolves into 1 mol Al_2OC, half of the N atoms may occupy 1 mol O atom positions in Al_2OC, and the other N atoms may occupy 1 mol C atom position therein. No additional vacancies are generated, so, the lattice distortion is relatively small. Furthermore, the solid solubility of AlN in Al_2OC can be as high as 50 mol.%. When the AlN content exceeds 15 mol%, the stability of the Al_2OC-AlN solid solution increases, and, as a result, Al_2OC is not easily decomposed into Al_4O_4C [19, 24-26]. According to the results mentioned above, it may be concluded that Al_2OC reasonably acts as the mesophase during AlN powder synthesis in the CRN process because of their extremely similar crystal structures.

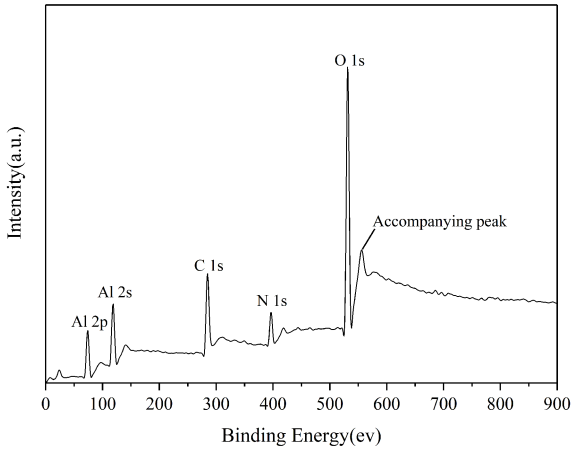

FIGURE 5 XPS spectrum of the dark grey AlN powder sample

Although the Al_2OC mesophase was identified by XRD in Figure 3, the proof is still inadequate, because the intensity of the Al_2OC diffraction peaks is rather weak. Other effective testing methods, e.g., XPS and TEM, were employed to determine the existence of the Al_2OC mesophase further. The whole XPS spectrum of the dark grey AlN powder sample is shown in Figure 5, containing the characteristic peaks of the Al,

N, C, and O elements. Among them, the C_{1S} and O_{1S} peaks are strong, indicating high C and O concentrations of the powder sample. During the XPS test, when the photoelectrons pass through the sample surface, inelastic collision occurs, resulting in energy loss. As a result, an accompanying peak exists on the spectrum, leading to the deviation of the peaks of the neighboring elements (Figure 5).

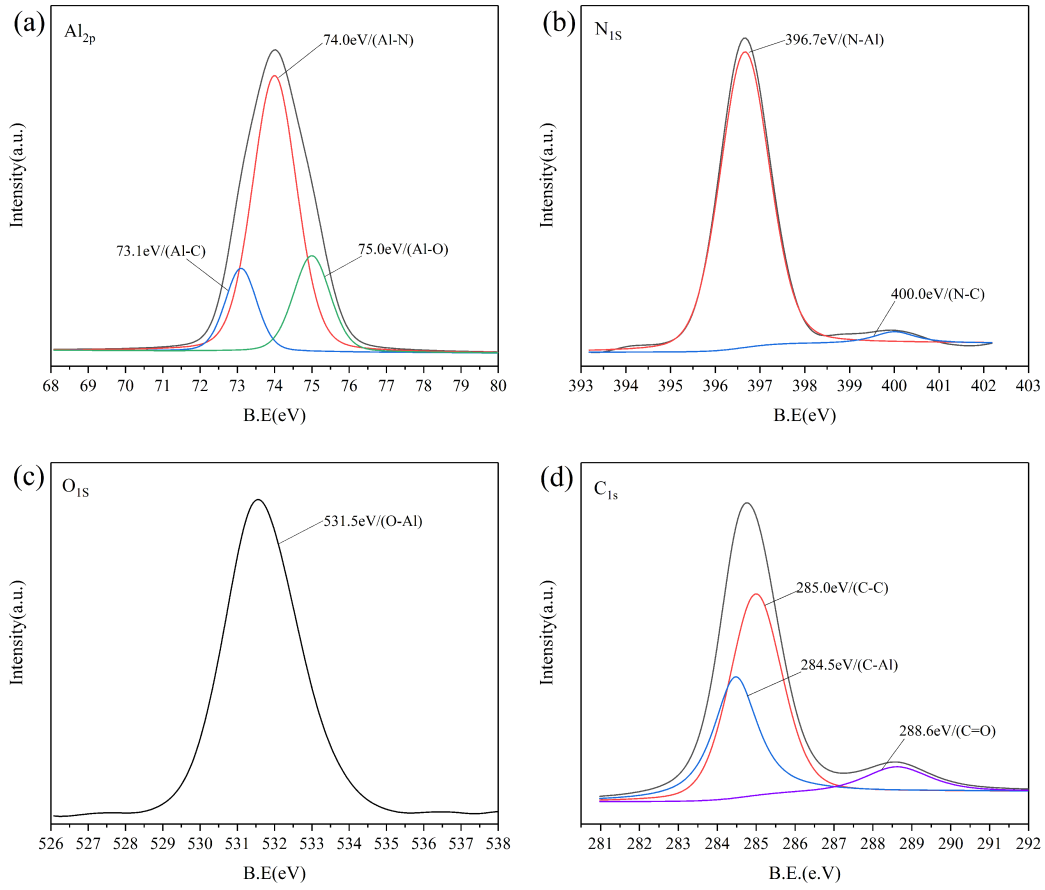

FIGURE 6 XPS spectra of Al_{2p}, N_{1s}, O_{1s} and C_{1s} of the dark grey AlN powder sample

TABLE 4 Standard binding energies between various elements [27]

Bond type	Al-N	Al-O	Al-C	N-Al	N-C	O-Al	C-C	C-Al	C=O
E_b/eV	73.9	74.3	72.9	396.2	400.2	531.6	284.8	284.4	287.8

After differentiating and imitating, the XPS spectra of the Al, N, O, and C elements of the dark grey AlN powder sample are shown in Figure 6. In Figure 6a, three peaks of binding energies of 75.0, 74.0, and 73.1 eV were disclosed, which are consistent

with the standard binding energies of the Al-O, Al-N, and Al-C bonds in Table 4, respectively. The N_{1S} peak in Figure 6b was divided into two peaks of binding energies of 396.7 and 400.0 eV, respectively, which were equal to the standard binding energies of the N-Al bond and N-C bonds in Table 4. The O_{1S} peak of a binding energy of 531.5 eV refers to the O-Al bond (Figure 6c). The C_{1S} peak in Figure 6d is trimodal, which corresponds to three single peaks of binding energies of 285.0, 284.5, and 288.6 eV, respectively, which are close to the standard binding energies of the C-C, C-Al and C=O bonds, respectively. In summary, in the XPS spectra of the AlN powder sample, the N-Al bond is associated with the N element in AlN, and the N-C bond corresponds to the C substance naturally adsorbed by AlN [28]. More importantly, the existence of the mesophase is confirmed indirectly by the O-Al, C-Al, and C=O bonds between two of the O, Al and C elements. In addition, most of the carbon in the sample exists in the form of a C-C bond, suggesting the elemental C exists in the dark grey AlN powder sample. The elemental C cannot be detected by XRD in Figure 3, due to its extremely low concentration and crystallinity.

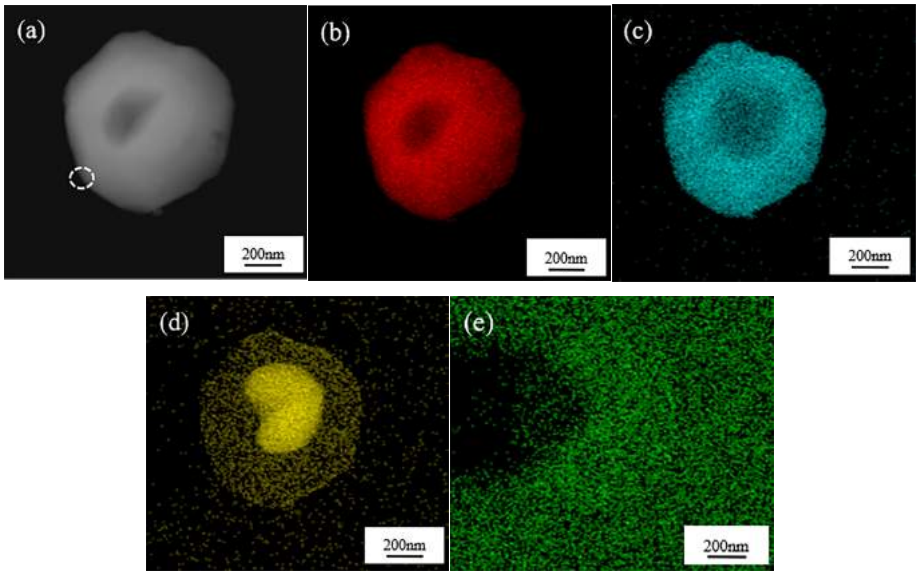

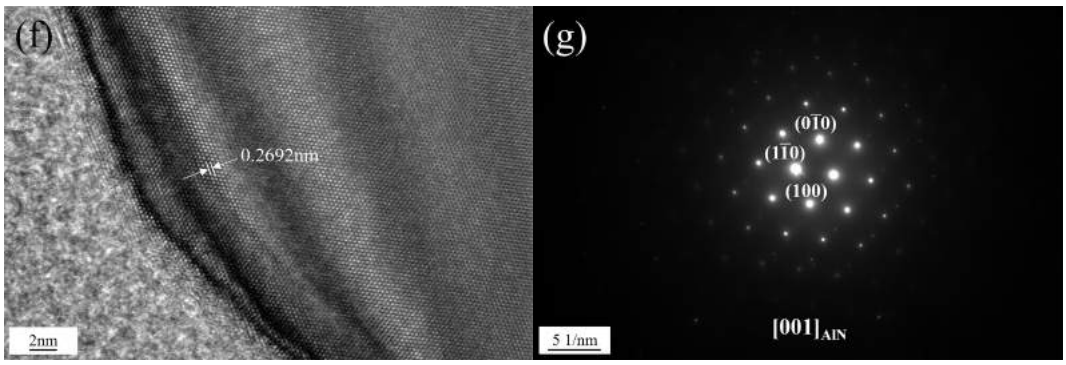

FIGURE 7 (a) TEM image and (b)-(e) Al, N, O, and C elemental mappings of the dark grey AlN powder sample, (f) and (g) HRTEM image and SAED pattern of the circle in (a)

Figure 7a-e are a TEM view and elemental mappings of a spherical AlN ultrafine particle of the dark grey AlN powder sample. A dark plaque in Figure 7a-e may be concave on the particle surface. As shown in Figure 7b-d, the Al and N contents are high throughout the particle, but the O element is generally concentrated in the central region of the particle of a shape like yolk. The HRTEM image and the selected area electron diffraction (SAED) spectrum of the edge of the particle are shown in Figure 7f and g. The planar spacing of 2.692 ± 0.059 Å in Figure 7f is very close to that of the AlN(100) plane (2.700 Å) [26]. In conjunction with the EDS results, the particle was determined to be AlN. During AlN powder synthesis in the CRN process, AlN nucleates on the Al_2O_3 particle surface. It gradually grows into a continuous AlN layer and encloses the residual Al_2O_3 core to form a core-shell structure [29]. The yolk-like region in Figure 7d is composed of not only residual Al_2O_3 but also the Al_2OC mesophase between the Al_2O_3 core and the AlN shell. To provide more conclusive evidence, the TEM of the dark grey AlN powder is shown next.

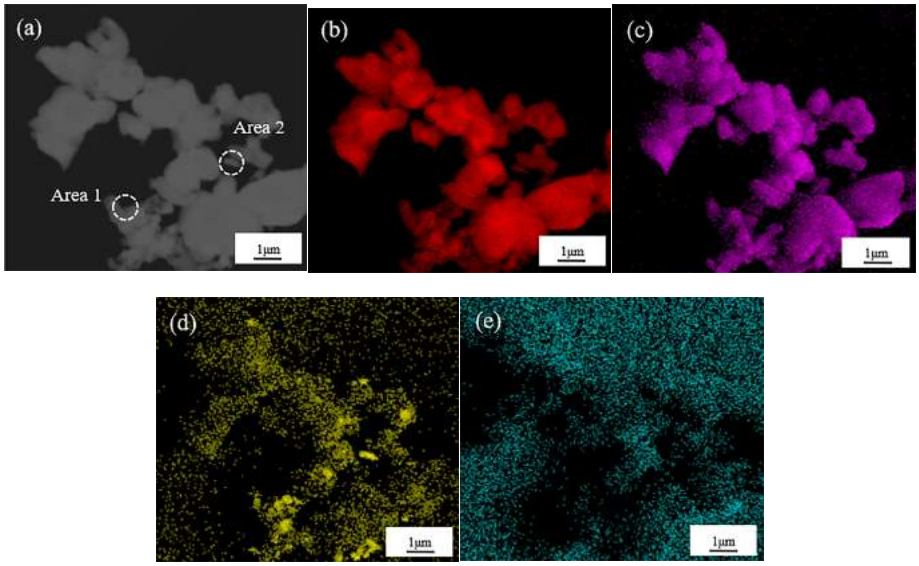

FIGURE 8 (a) TEM image and elemental mappings of the dark grey AlN powder sample (b) Al; (c) N; (d) O; (e) C

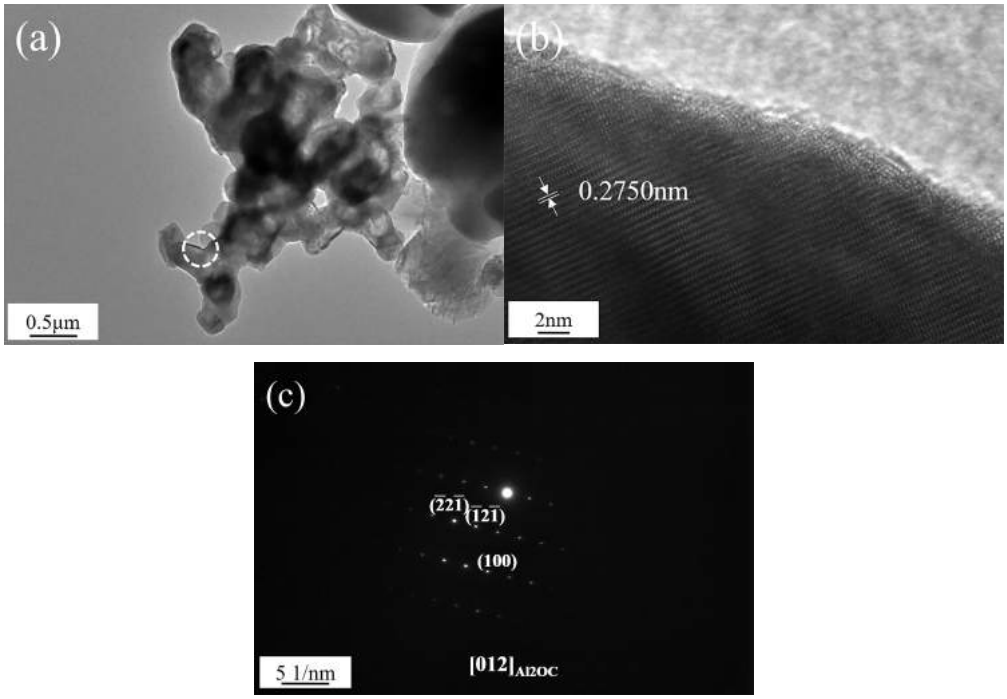

FIGURE 9 (a), (b) (HR)TEM images of the dark grey AlN powder sample; (c) SAED spectrum

In Figure 8a, the O-enriched micro-zones are located by the EDS results in Figure 8b-e. Among them, Area 1 is rich in Al, O, and C elements, and Area 2 is composed of

only Al and O elements. Focusing on Area 1 in Figure 8a, its high-magnification TEM image is shown in Figure 9a. In the HRTEM image of the circle in Figure 9a, planar spacing of 2.750 ± 0.029 Å was determined, which was very close to that of the Al_2OC(100) (2.759 Å) [24] (Figure 9b). Similarly, the SAED spectrum of the same area in Figure 9c also indicates the Al_2OC mesophase. By the same method, Area 2 in Figure 8a could be determined as an unreduced Al_2O_3 particle.

In summary, the formation of the Al_2OC mesophase has been confirmed in the CRN-synthesized AlN powder when the involved solid-state reaction is incompletely performed. The Al_2OC mesophase brings the C and O impurities into the AlN powder together, resulting in degraded quality of the powder. Next, the formation and transformation thermodynamics of the Al_2OC mesophase of AlN powder in the CRN process can be further deduced.

3.3 Thermodynamic calculations

Under the conditions of the calcining temperature, T = 1973.15 K (1700 °C), and the atmospheric pressure in the synthesis furnace, P_t = 101.667 kPa (1 atm), the equilibrium constant Q of each reaction in the CRN process was calculated, based on the relevant thermodynamic data. Then, a function expression on the CO(g) partial pressure in the synthesis furnace, P_{CO}, was deduced to determine the boundary regions between two different phases. Last, the isothermal section of the AlN-Al_2O_3-Al_2OC ternary phase diagram at 1973.15 K was derived.

It is known that the total reaction for AlN powder synthesis by CRN is as follows:

$$Al_2O_3(s) + 3C(s) + N_2(g) = 2AlN(s) + 3CO(g) \quad (2)$$

By means of the thermochemical data in Ref. [30], an equation concerning Gibbs free energy difference of the reaction, ΔG_1, was derived (detailed in the Appendix):

$$\Delta G_1 = 708.101 - 0.374T + 2.303RT\log Q_1 \quad <1>$$

where R is the gas constant, 8.314×10^{-3} kJ/(K·mol); T is the reaction temperature, K; Q_1 is the equilibrium constant of reaction 2, $Q_1=(P_{CO}/P_\theta)^3/(P_{N2}/P_\theta)$; P_{CO} and P_{N2} are the CO/N_2 equilibrium partial pressures in the synthesis furnace, kPa; P_θ is a constant equal to 100 kPa.

When reaction 2 is in an equilibrium state ($\Delta G_1 = 0$), P_{N2} can be expressed as:

$$logP_{N2} = 3logP_{CO} - 4.765 \quad <2>$$

According to the results reported by Lefort et al. [31], the carbothermal reduction reaction to form the Al_2OC mesophase is described as:

$$Al_2O_3(s) + 3C(s) = Al_2OC(s) + 2CO(g) \quad (3)$$

Based on the relevant thermodynamic data in Ref. [30] and HSC thermodynamic software data (Al_2OC) [32], an equation on Gibbs free energy difference of reaction (3), ΔG_2, was deduced:

$$\Delta G_2 = 776.802 - 0.354T + 2.303RT\log Q_2 \quad <3>$$

where Q_2 is the equilibrium constant of reaction (3), $Q_2=(P_{CO}/P_\theta)^2$.

When reaction 3 is in equilibrium at 1973.15 K, then

$$logP_{CO} = 0.973 \quad <4>$$

According to Ref. [31], when reaction 3 takes place, Al(g) exists and reacts with CO, resulting in the formation of the Al_2OC mesophase. However, as the P_{CO} in the

atmosphere is decreased, reaction 4 goes on to allow for the Al_2OC mesophase to decompose to form A1(g):

$$Al_2OC(s) = 2A1(g) + CO(g) \quad (4)$$

A1(g) then reacts with N_2 in the atmosphere to form AlN:

$$2A1(g) + N_2(g) = 2A1N(s) \quad (5)$$

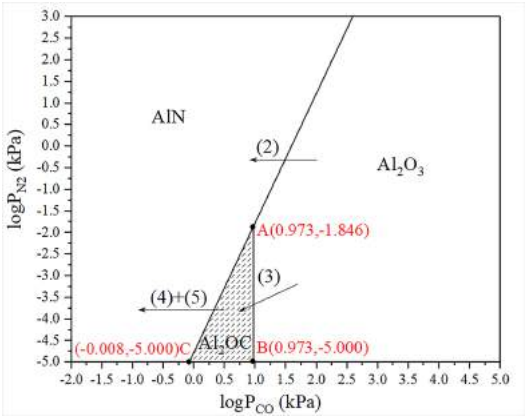

FIGURE 10 Calculated partial equilibrium phase diagram at 1973.15 K

As shown in Figure 10, in the plane coordinate system with $logP_{CO}$ as the x-axis and $logP_{N2}$ as the y-axis, two lines of AB and AC were constructed, based on Eqs. 2 and 4, respectively. The isothermal section of the AlN-Al_2O_3-Al_2OC ternary phase diagram at 1973.15 K was obtained in which point A is the three-phase equilibrium point of (AlN + Al_2O_3 + Al_2OC) ($P_{N2} = 10^{-1.846}$ kPa, $P_{CO} = 10^{0.973}$ kPa). Points A, B ($P_{N2} = 10^{-5.000}$ kPa, $P_{CO} = 10^{0.973}$ kPa) and C ($P_{N2} = 10^{-5.000}$ kPa, $P_{CO} = 10^{-0.008}$ kPa) show an ABC triangular region, which is the single-phase region of the Al_2OC mesophase. With P_{N2} above $10^{-1.846}$ kPa (point A), as the partial pressure of CO decreases, reaction 2 is preferential, and Al_2O_3 is converted to AlN. When the N_2 pressure was below $10^{-1.846}$ kPa and the P_{CO} was as low as $10^{0.973}$ kPa, reaction 3 was promoted to form the Al_2OC mesophase. When the P_{N2} in the synthesis furnace was

low as 10^{-5} kPa, the Al_2OC mesophase was stable in the P_{CO} range of $10^{-0.008}$-$10^{0.973}$ kPa. The results above are consistent with the result that the Al_2OC mesophase is produced in the P_{CO} range of 1-10 kPa at 2100 K and an atmospheric total pressure of 100 kPa [31]. When the P_{CO} is further decreased to the left of the AC line segment, reactions 4 and 5 are favored, and the Al_2OC mesophase decomposes to form A1(g), which reacts with N_2 in the atmosphere to form AlN.

In summary, to avoid the formation of the Al_2OC mesophase and/or eliminate the formed Al_2OC mesophase in the CRN process of the AlN powder, there are achievable routes i.e., increasing P_{N2} and reducing P_{CO} in the synthesis furnace. In this situation, reaction 2 is thermodynamically favored, meanwhile, the formed Al_2OC mesophase decomposes into AlN.

3.4 Elimination of the Al_2OC mesophase

According to the thermodynamic calculations in section 3.3, the P_{N2} in the synthesis furnace can be increased and the P_{CO} in the synthesis furnace can be decreased by increasing the N_2 flow in the synthesis furnace. Therefore, reactions 2, 4, and 5 take place in the positive direction. The conversion of Al_2O_3 to AlN and the decomposition of the formed Al_2OC mesophase are promoted. To verify these assumptions, experiments synthesizing AlN powder in the CRN process at different N_2 flow rates were carried out. Table 5 shows the O, N and C contents of the AlN powder synthesized in the CRN process at different N_2 flow rates. As the N_2 flow rate of 250 L/min was employed previously, the O and C contents of the AlN powder were

the highest, and the N content of the AlN powder was the lowest, after calcinating at 1700 °C for 12 h and then decarburizing and pulverizing, resulting from the formation of the Al_2OC mesophase and/or inadequate reduction of Al_2O_3 during the CRN reaction. As the N_2 flow rate increased to 320 and 400 L/min, the O and C contents of the AlN powder gradually decreased, while the N content of the AlN powder increased significantly. That is, by adjusting the N_2 flow rate during AlN powder synthesis in the CRN process, the concentrations of the O and C impurities of the AlN powder fabricated in batch quantities could be controlled at a very low level, which were slightly higher than those of grade H-AlN powder synthesized by the same CRN process from Tokuyama, Japan (O content: 0.8 wt%, C content: 280 ppm) [33].

TABLE 5 O, N and C contents of the AlN powder synthesized at different N_2 flow rates

Sample	N_2 flow rate/(L/min)	O/(wt%)	N/(wt%)	C/(ppm)
1	250	1.02	33.46	627
2		0.98	33.49	653
3		1.04	33.45	701
Ave.		1.01	33.47	660
4	320	0.87	33.52	512
5		0.88	33.52	539
6		0.85	33.50	558
Ave.		0.87	33.51	536
7	400	0.81	33.55	450
8		0.85	33.52	463
9		0.85	33.51	456
Ave.		0.84	33.53	456

The optimal process for AlN powder synthesis using the CRN process in batch quantity was finally determined, i.e., calcining at 1700 °C for 12 h with an N_2 flow rate of 400 L/min. The other technical parameters in the CRN process were unchanged.

3.5 Properties of the AlN Ceramics

TABLE 6 O, N and C compositions of the AlN powders employed to fabricate the AlN ceramics

Sample	O/(wt%)	N/(wt%)	C/(ppm)
P1	0.84	33.53	456
P2	0.95	33.54	521
P3	1.01	33.47	660
P4	1.18	33.27	653
P5	1.46	33.30	827

As mentioned above, the AlN powders of different O, N and C contents were synthesized by adjusting the N_2 flow rate in the atmosphere of the synthesis furnace. Five types of the AlN powders were chosen to fabricated the AlN ceramics (Table 6) to investigate the effects of the impurity contents of the AlN powder, especially the O content, on the microstructures and properties of the AlN ceramics.

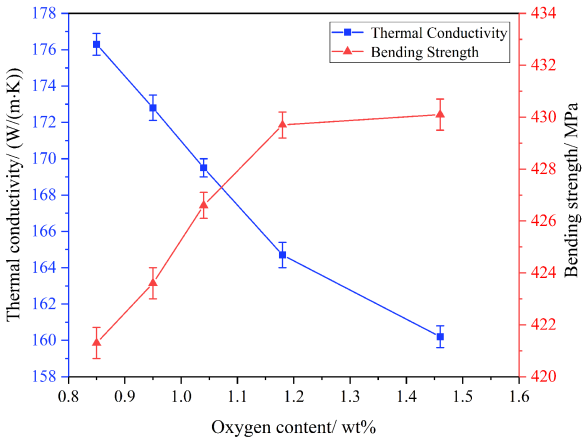

FIGURE 11 Relationships between the thermal conductivities and bending strengths of the AlN ceramics and the O content of the AlN powders

The densities of the AlN ceramics, named S1-S5, corresponding to the P1-P5 AlN powders, respectively, are approximately equal (about 3.3 g/cm^3), but the thermal conductivities and bending strengths of them are significantly different. As shown in Figure 11, as the O content of the AlN powder decreased, the thermal conductivities of the AlN ceramics monotonously increase. When the O content of the AlN powder is less than 1.2 wt%, the thermal conductivities of the AlN ceramics increase more dramatically. On the contrary, the bending strengths of the AlN ceramics keep almost constant, as the O content of the AlN powder decreased from 1.46 wt% to 1.2 wt%. And then, they drop accelerately, as the O content of the AlN powder decreased from 1.2 wt% to 0.84 wt%. Definitely, the properties of the AlN ceramics are very sensitive to the O content of the AlN powders.

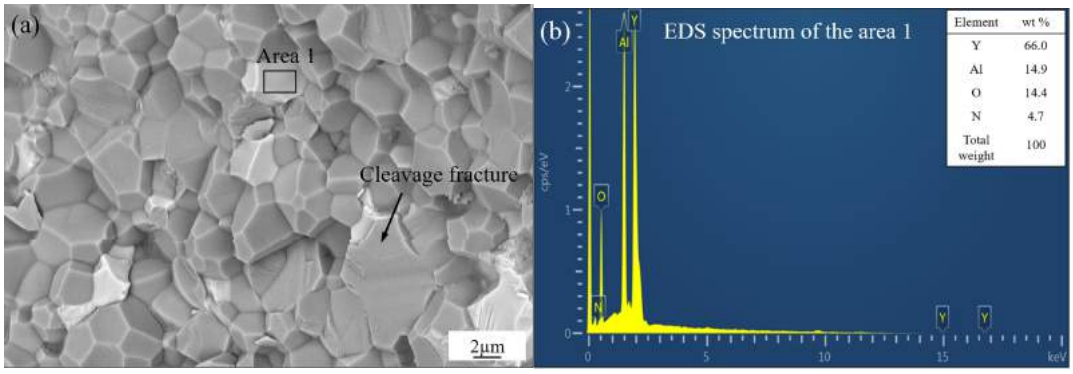

FIGURE 12 (a) Back scattering electronic SEM image and (b) microzone EDS spectrum of the AlN ceramic S1

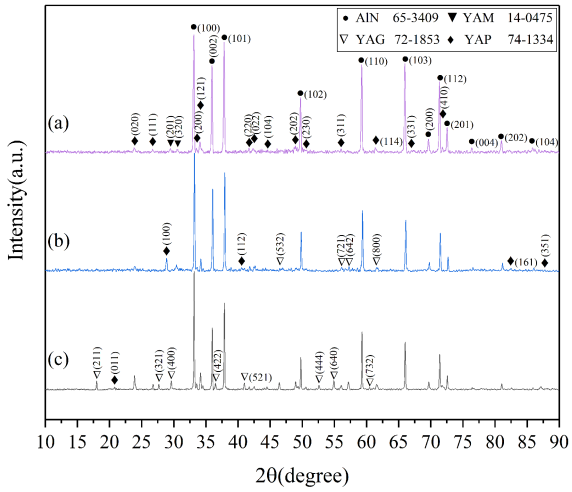

FIGURE 13 XRD patterns of the AlN ceramics (a) S1; (b) S3; (c) S5

As shown in Figure 12a, the AlN ceramic S1 is dense without any pores. The AlN grains are well-developed of a grain size about 3-5 μm. The bending fracture of the AlN ceramic mainly takes place intergranularly, but the cleavage fracture of couples of large AlN grains also occurs. Several bright grains in Figure 12a are situated at the AlN grain boundaries, the EDS testing result shows that they contain high Y, Al and O contents (Figure 12b). During sintering the AlN ceramics, the O impurity in the AlN powder reacts with Y_2O_3 to form an Al_2O_3-Y_2O_3 melt, promoting the rapid densification of the AlN ceramics. The melt is then transformed into YAP ($YAlO_3$), YAM ($Y_4Al_2O_9$) and YAG ($Y_3Al_5O_{12}$) in the cooling process of the AlN ceramics [34, 35]. As shown in Figure 13a, two oxide phases, YAP and YAM, are formed in the AlN ceramic S1, and the intensities of the diffraction peaks of them are rather weak, because the O content of the AlN powder P1 is the lowest. In the AlN ceramics S3 and S5, YAG is also detected by XRD, besides YAP and YAM. As the O content of the AlN powder increased from P3 to P5, the intensities of diffraction peaks of the three oxides increase, indicating more YAP, YAM and YAG in the AlN ceramics (Figure

13b, c). These oxides are distributed along the AlN grain boundaries to form a strong interfacial bond with the AlN grains, resulting in the significant increase of the bending strength of the AlN ceramics [36]. However, the thermal conductivities of these oxides are very low, e.g., AlN: 320 W/(m·K), YAG: 10.2 W/(m·K) [37], the thermal conductivity of the AlN ceramics is apparently decreased with increasing the amount of the oxides.

In summary, the comprehensive properties of the AlN ceramics are excellent, using the high-quality AlN powder synthesized in this work as raw materials, i.e., the thermal conductivity 176.3 W/(m·K), and the bending strength 421.3 MPa. They are comparable to those of the internationally-advanced SH-15 grade AlN ceramics (184 W/(m·K), 357 MPa, respectively) and SH-30 grade ones (174 W/(m·K), 511 MPa, respectively) developed by Tokuyama, Japan [38].

4 Conclusions

1. The dark gray AlN powder particles were nearly spherical with a nonuniform microzone composition distribution. The existence of the Al_2OC mesophase in the CRN-synthesized AlN powder was first identified by XRD, XPS, and TEM investigations. A small amount of the Al_2OC mesophase and residual C and Al_2O_3 were detected in the AlN powder, resulting in high concentrations of O and C impurities in the AlN powder.

2. During AlN powder synthesis in the CRN process, a core-shell structure composed of the Al_2O_3 core wrapped by the AlN shell was formed with the Al_2OC mesophase at

the AlN/Al_2O_3 interface. The Al_2OC mesophase is an incomplete reduction product of the Al_2O_3 particles and has a highly similar crystal structure to AlN. It is also one of the major sources of C and O impurities of the AlN powder synthesized in the CRN process.

3. Based on the thermodynamic calculations, the isothermal section of the AlN-Al_2O_3-Al_2OC ternary phase diagram at 1973.15 K was constructed. When the P_{N2} was lower than $10^{-1.846}$ kPa, there was an ABC triangular region contained within, corresponding to the Al_2OC single phase region. When the P_{N2} was as low as 10^{-5} kPa, the Al_2OC mesophase was stable in the P_{CO} range of $10^{-0.008}$-$10^{0.973}$ kPa. In contrast, the Al_2OC mesophase was not stable and decomposed into AlN by increasing the P_{N2} and/or lowering the P_{CO} in the synthetic furnace.

4. The optimal process for AlN powder synthesis in the CRN process was determined as follows: calcination at 1700 °C for 12 h with a N_2 flow rate of 400 L/min, while the other technical parameters were unchanged. Under these conditions, the AlN powder synthesized in batch quantities was light grey with high N content and low O and C contents. At these conditions, a high-quality AlN powder was stably produced.

5. The O content of the AlN powder has great influences on the thermal conductivity and strength of the AlN ceramics. The AlN ceramics made of the AlN powder of the O content as low as 0.84 wt% have a thermal conductivity of 176.3 W/(m·K) and a bending strength of 421.3 MPa.

Acknowledgements

This work is financially supported by Science and Technology Research Project of Anhui Province, China (Grant No. 1604a0902162).

ORCID

Xin Wei, https://orcid.org/0000-0001-5348-6006

Wenming Tang, https://orcid.org/0000-0002-7493-9876

References

[1] Shang QS, Wang ZJ, Li J, Zhou GH, Zhang HL, Wang SW. Gel-tape-casting of aluminum nitride ceramics. J. Adv. Ceram. 2017;6(1);67-72. https://doi.org/10.1007/s40145-016-0211-3.

[2] Cao Y, Xu HX, Zhan J, Zhang H, Wei X, Wang JM, Cui S, Tang WM. Experimental and modeling studies on the microstructures and properties of oxidized aluminum nitride ceramic substrates. J. Mater. Eng. Perform. 2018;27;3297-3303. https://doi.org/10.1007/s11665-018-3415-6.

[3] Xu FM, Zhang ZJ, Shi XL, Tan Y, Yang JM. Effects of adding yttrium nitrate on the mechanical properties of hot-pressed AlN ceramics. J. Alloys. Compds. 2011;509(35);8688-8691. https://doi.org/10.1016/j.jallcom.2011.05.110.

[4] Wang Q, Kuang JL, Jiang P, Cao WB. Carbothermal synthesis of spherical AlN particles using sucrose as carbon source. Ceram. Int. 2018;44(3);3480-3483. https://doi.org/10.1016/j.ceramint.2017.11.056.

[5] Chu AM, Qin ML, Rafi-ud-din, Jia BR, Lu HF, He XB, Qu XH. Effect of aluminum source on the synthesis of AlN powder from combustion synthesis precursors. Mater. Res. Bull. 2012;47(9);2475-2479. http://dx.doi.org/10.1016/j.materresbull.2012.05.014.

[6] Fu L, Qiao L, Zheng JW, Ying Y, Li WC, Che SL, Yu J. Phase, microstructure and sintering of aluminum nitride powder by the carbothermal reduction-nitridation process with Y_2O_3 addition. J. Eur. Ceram. Soc. 2018;38(4);1170-1178. http://dx.doi.org/10.1016/j.jeurceramsoc.2017.10.029.

[7] Zhang PG, Wang KY, Guo SM. Large-scale synthesis of AlN nanofibers by direct nitridation of aluminum. Ceram. Int. 2010;36(7);2209-2213. https://doi.org/10.1016/j.ceramint.2010.05.024.

[8] Falamaki C, Tari MH, Ebadzadeh T. A new route for the direct synthesis of Al_2O_3/SiC nanopowder mixtures by the carbothermal reduction of parent oxides. AIChE Journal. 2010;56(5);1372-1382. https://doi.org/10.1002/aic.11973.

[9] Hsieh CY, Lin CN, Chung SL, Cheng J, Agrawal DK. Microwave sintering of AlN powder synthesized by a SHS method. J. Eur. Ceram. Soc. 2007;27(1);343-350. https://doi.org/10.1016/j.jeurceramsoc.2006.03.003.

[10] Kwon HT, Bukhovko MP, Mahamulkar S, Sulmonetti T, Min B, Almas Q, Malek A, Li LW, Agrawal PK, Jones CW. Sol–gel derived CeO_2/α-Al_2O_3 bilayer thin film as an anti-coking barrier and its catalytic coke oxidation performance. AIChE Journal. 2018;64(11);4019-4026. https://doi.org/10.1002/aic.16383.

[11] B. Forslund, J. Zheng. Carbothermal synthesis of aluminium nitride at elevated nitrogen pressures - Part I Effect of process parameters on conversion rate. J. Mater. Sci. 1993;28;3125-3131. http://doi.org/10.1007/BF00354225.

[12] Yu WZ, Yang B, Chen XM, Jiang WL, Yu QC, Xu BQ. Thermodynamic calculation and experimental investigation on the products of carbothermal reduction of Al_2O_3 under vacuum. Vacuum. 2012;86(12);2005-2009. https://doi.org/10.1016/j.vacuum.2012.04.017.

[13] Qin ML, Dua XL, Wang J, Humail IS, Qua XH. Influence of carbon on the synthesis of AlN powder from combustion synthesis precursors. J. Eur. Ceram. Soc.

2009;29(4);795-799. https://doi.org/10.1016/j.jeurceramsoc.2008.07.019.

[14] Harris JH, Youngman RA, Teller RG. On the nature of the oxygen-related defect in aluminum nitride. J. Mater. Res. 1990;5;1763-1773. http://doi.org/10.1557/JMR.1990.1763.

[15] AlShaikhi A, Srivastava GP. Role of additives in enhancing the thermal conductivity of AlN ceramics. J. Phys. D: Appl. Phys. 2008;41;185407. http:// doi.org/10.1088/0022-3727/41/18/185407.

[16] Foster LM, Long G, Hunter MS. Reactions between aluminum oxide and carbon the Al_2O_3-Al_4C_3 phase diagram. J. Am. Ceram. Soc. 1956;39(1);1-11. http://doi.org/ 10.1111/j.1151-2916.1956.tb15588.x.

[17] Yan HW, Cannon WR, Shanefield DJ. Evolution of carbon during burnout and sintering of tape-cast Aluminum Nitride. J. Am. Ceram. Soc. 1993;76(1);166-172. http:// doi.org/10.1111/j.1151-2916.1993.tb03702.x.

[18] Liu SC, Ye F, Liu LM, Liu Q, Li JY. Preparation of Aluminum Nitride Ceramics by aqueous tape casting. Mater. Manuf. Process. 2015;30(5);605-610. http:// doi.org/10.1080/10426914.2014.973592.

[19] Amma EL, Jeffrey GA. Study of the wurtzite-type compounds. V. structure of aluminum oxycarbide, Al_2CO; A short-range wurtzite-type superstructure. J. Chem. Phys. 1961;34;252-259. http:// doi.org/10.1063/1.1731572.

[20] Jeffrey GA, Slaughter M. The structure of aluminum tetroxycarbide. Acta Crystallogr. 1963;16;177-184. http:// doi.org/10.1107/S0365110X63000451.

[21] Yokokawa H, Dokiya M, Fujishige M, Kameyama T, Ujiie S, Fukuda K. X-ray

powder diffraction data for two hexagonal aluminum monoxycarbide phases. J. Am. Ceram. Soc. 1982;65;40-41. http://doi.org/10.1111/j.1151-2916.1982.tb10394.x.

[22] Jeffrey GA, Wu VY. The structure of the aluminum carbonitrides II. Acta Crystallogr. 1966;20;538-547. http://doi.org/10.1107/S0365110X66001208.

[23] Qiu CA, Metselaar R. Phase relation in the aluminum carbide-aluminum nitride-aluminum oxide system. J. Am. Ceram. Soc. 1997;80(8);2013-2020. http://doi.org/10.1111/j.1151-2916.1997.tb03085.x.

[24] Henry JL, Russel JH, Kelly HJ. The system Al_4C_3-AlN-Al_2O_3: powder forming and sintering behavior, phase identification, and refractory composition properties. In: U. S. Bu. Mines (ed.), report of investigations 7320, U.S. Dept. of the Int. Library. Washington: D.C., 1969:24.

[25] Kroger FA and Vink HJ. Relations between the concentrations of imperfections in crystalline solids. Solid State Phys. 1956;3;307-435. http://doi.org/10.1016/S0081-1947(08)60135-6.

[26] Lihrmann JM, Zambetakis T, Daire M. High-temperature behavior of the aluminum oxycarbide Al_2OC in the system Al_2O_3–Al_4C_3 and with additions of aluminum nitride. J. Am. Ceram. Soc. 1989;72(9);1704-1709. http://doi.org/10.1111/j.1151-2916.1989.tb06306.x.

[dataset] [27] NIST X-ray Photoelectron Spectroscopy Database. NIST XPS Database, selected element search menu, NIST Standard Reference Database 20, V4.1. 2019. https://srdata.nist.gov/xps/selEnergyType.aspx.

[28] Liu W, Wang ZW, Yang QD, Wei JT. AFM and XPS analysis of silicon-based

aluminum nitride films. Piezoelectrs. Acoustoopt. 2007;29(6);723-725 (In Chinese). https://doi.org/10.3969/j.issn.1004-2474.2007.06.031.

[29] O'Donnell RG, Trigg MB. The mechanism of conversion of Al_2O_3, to AlN via carbothermal synthesis. Micron. 1994;25(6);575-579. https://doi.org/10.1016/0968-4328(94)90019-1.

[30] Barin I, Platzki G. Thermochemical Data of Pure Substances (Third ed). VCH Verlagsgesellschaft mbH, Weinheim, 1995.

[31] Lefort P, Tetard D, Tristant P. Formation of aluminium carbide by carbothermal reduction of alumina: Role of the gaseous aluminium phase. J. Eur. Ceram. Soc. 1993;12(2);123-129. https://doi.org/10.1016/0955-2219(93)90132-B.

[dataset] [32] A. Roine. HSC Chemistry 6: H, S, C and G Diagrams, HSC Data, v6, 2006.

[33] Tokuyama Co. Ltd. High purity aluminum nitride powder. https://www.tokuyama.co.jp/products/specialtyproducts/aln_powder_granules.html. 2019 (accessed Sept. 28, 2019).

[34] Huang D, Tian ZB, Cui W, Gao LQ, Liu Z, Diao XG. Effects of Y_2O_3 and yttrium aluminates as sintering additives on the thermal conductivity of AlN ceramic substrates. Ceram. Int. 2018;44(16);20556-20559. https://doi.org/10.1016/j.ceramint.2018.07.178.

[35] Neher R, Herrmann M, Fabrichnaya O, Pavlyuchkov D, Seifert HJ. Liquid phase formation in the system AlN–Al_2O_3–Y_2O_3. Part I: Experimental investigations. J. Eur. Ceram. Soc. 2013;33(13-14);2447-2455.

https://doi.org/10.1016/j.jeurceramsoc.2013.04.028.

[36] Yao YJ, Qiu T. Effect of Y_2O_3 and Dy_2O_3 on microstructure and mechanical behaviors of Aluminum Nitride ceramics. J. Rare Earths. 2006;24(1);239-243. https://doi.org/10.1016/S1002-0721(07)60370-6.

[37] Sato Y, Taira T. Comparison of thermal conductivity in YAG between polycrystalline ceramics and single crystals. Frontiers in Optics. 2006. https://doi.org/10.1364/FIO.2006.FMK2.

[38] Tokuyama Co. Ltd. Aluminum Nitride Ceramic. https://www.tokuyama.co.jp/products/specialtyproducts/aln_ceramics.html. 2020 (accessed Jan. 18, 2020).